Red cells' dynamic morphologies govern blood shear thinning under microcirculatory flow conditions

Luca Lanotte[a], Johannes Mauer[b], Simon Mendez[c], Dmitry A. Fedosov[b], Jean-Marc Fromental[d], Viviana Claveria[a], Franck Nicoud[c], Gerhard Gompper[b], and Manouk Abkarian[a,1]

[a]Centre de Biochimie Structurale, CNRS UMR 5048, INSERM UMR 1054, University of Montpellier, 34090 Montpellier, France; [b]Institute of Complex Systems and Institute for Advanced Simulation, Forschungszentrum Jülich, 52425 Juelich, Germany; [c]Institut Montpelliérain Alexander Grothendieck, UMR 5149 051, University of Montpellier, 34095 Montpellier, France; and [d]Laboratoire Charles Coulomb, CNRS UMR 5587, University of Montpellier, 34095 Montpellier, France

Edited by David A. Weitz, Harvard University, Cambridge, MA, and approved October 11, 2016 (received for review May 19, 2016)

Blood viscosity decreases with shear stress, a property essential for an efficient perfusion of the vascular tree. Shear thinning is intimately related to the dynamics and mutual interactions of RBCs, the major component of blood. Because of the lack of knowledge about the behavior of RBCs under physiological conditions, the link between RBC dynamics and blood rheology remains unsettled. We performed experiments and simulations in microcirculatory flow conditions of viscosity, shear rates, and volume fractions, and our study reveals rich RBC dynamics that govern shear thinning. In contrast to the current paradigm, which assumes that RBCs align steadily around the flow direction while their membranes and cytoplasm circulate, we show that RBCs successively tumble, roll, deform into rolling stomatocytes, and, finally, adopt highly deformed polylobed shapes for increasing shear stresses, even for semidilute volume fractions of the microcirculation. Our results suggest that any pathological change in plasma composition, RBC cytosol viscosity, or membrane mechanical properties will affect the onset of these morphological transitions and should play a central role in pathological blood rheology and flow behavior.

blood rheology | red blood cell | cell dynamics | blood simulation

RBCs are the main cellular component of whole blood (WB). About a thousand times more concentrated than white blood cells and platelets, the volume fraction of RBCs or their hematocrit (Ht) is as high as 45%. Local dynamics and interactions of RBCs govern blood rheology and control proper perfusion of the entire vascular tree. In particular, WB exhibits a strong shear-thinning behavior in shear flow (1, 2) that is determined by the aggregability and deformability of RBCs (3), because the suspending plasma behaves essentially as a Newtonian fluid with a constant shear viscosity of about 1.2 cP at 37°C (1, 4). Macromolecules dispersed in the plasma, such as fibrinogen, induce an attractive force between RBCs, leading to their aggregation (5). Because RBCs have a biconcave disk-like shape at rest, they form long floppy rouleaux structures that can reversibly and continuously break down to single flowing discocytes for increasing shear rates up to tens of seconds^{-1} (6, 7). This change in microstructure is indeed accompanied by a strong viscosity drop from ~ 100 cP down to about ~ 10 cP (3). However, for shear rates between 10 and $1{,}500$ s^{-1}, which are common in the microcirculation (8, 9), only deformability and dynamics of RBCs can account for a further fourfold decrease in WB viscosity down to values as low as $2-3$ cP (3). This value strongly depends on the Ht and the viscosity of RBC hemoglobin cytoplasm, which is around 5 cP at 37°C (10).

The link between cellular deformability and shear thinning remains unsettled, even though it is crucial for understanding blood flow both in health and disease: Altered RBC deformability (11) is correlated with impaired perfusion, increase in blood viscosity, and vasoocclusion in microcirculatory disorders such as diabetus mellitus or hemoglobinopathies such as sickle cell anemia. Observations of RBC dynamics in microtubes (12) and rheoscopes (13) realized during the 1970s and 1980s have led to the foundation of the current paradigm for shear thinning, supporting an emulsion analogy for blood rheology inherited from the 1960s (1, 2). Although at low shear stresses (less than about 0.05 Pa) single RBCs flip like a coin, they reach a steady orientation for increasing flow strength (13, 14) allowed by a tank-tread-like circulation of their membrane (13). Such droplet-like behavior should effectively assist the flow by minimizing disturbances to streamlines and has been successfully used to deduce some mechanical properties of RBC membrane in dilute conditions (15, 16). However, steady tank treading occurs only when RBCs are dispersed into a viscous aqueous solution (often of dextran polysaccharides), which is several times more viscous than the inner cytoplasm. Such a viscous environment around single cells is supposed to mimic the effective high-shear-rate viscosity of the crowded conditions present in WB (17). Therefore, the shear-thinning paradigm is rooted in RBCs' ability to tank-tread whatever the Ht in response to high shear stresses (7).

Recent experiments realized on dilute RBC suspensions with outer viscosities similar to that of the hemoglobin-rich cytoplasm have demonstrated, however, that the solid-like tumbling motion is not replaced by tank treading for increasing shear rates, but rather by a typical solid rolling motion, where the axis of symmetry of the discocyte lies in the direction of vorticity (18). Even for shear stresses up to 0.5 Pa no fluidization of the membrane was observed, demonstrating the important role the inner-to-outer viscosity ratio λ plays on local dynamics. In fact, plasma viscosity under physiological conditions is about five times smaller than that of RBCs cytosol. New studies are thus required to investigate RBCs' local dynamics at such low viscosity conditions and high shear rates.

Significance

Our work reveals rich RBCs' dynamic morphologies which govern blood shear thinning under microcirculatory flow conditions, contrary to the current paradigm assuming steady RBC orientation and membrane circulation. Our results suggest that any pathological change in RBCs' local rheology will impact the onset of these morphological transitions and should play a key role in pathological blood flow.

Author contributions: L.L. and J.-M.F. ran rheometry experiments; L.L. realized microfluidic observations; L.L. and V.C. did image analysis; J.M., S.M., D.A.F., F.N., and G.G. performed simulations; L.L., J.M., and S.M. analyzed data; and L.L., J.M., S.M., D.A.F., G.G., and M.A. wrote the paper.

The authors declare no conflict of interest.

This article is a PNAS Direct Submission.

[1]To whom correspondence should be addressed. Email: Manouk.Abkarian@univ-montp2.fr.

This article contains supporting information online at www.pnas.org/lookup/suppl/doi:10.1073/pnas.1608074113/-/DCSupplemental.

In this work, we explore the shape and dynamics of RBCs in the range of shear rates $\dot{\gamma}$ between 10 and 1,500 s^{-1} and Hts from 5 up to 45% relevant for the microcirculation (8, 9). We correlate RBCs' dynamical morphologies with blood shear thinning measured by rheometry. Using microfluidics, we demonstrate that RBCs show unexpected dynamics characterized by rotating polylobed shapes, with no clear tank treading of their membrane. Experimental results are corroborated by two different 3D simulation techniques: a continuum approach (19) based on the finite-volume method and a mesoscopic approach (20) based on the smoothed dissipative particle dynamics (SDPD) method (21). We discuss the implication of this work for microcirculatory flow and reinterpret the classical shear-thinning conjecture.

Results

Morphology of RBCs in Simple Shear Flow. We first explore the morphologies of single RBCs at 37°C subjected to a simple shear flow in a range of $\dot{\gamma}$ between 10 s^{-1} and 2,000 s^{-1} using a cone-and-plate rheometer. Cells are quickly hardened with an aldehyde treatment while flowing (see protocol in *Materials and Methods*). Samples of these hardened RBCs (HRBCs) are then withdrawn from the plate of the rheometer and visualized by bright-field (BF) and confocal microscopy after fluorescent dyeing of their membranes. Typical images of the fixed shapes are shown in Fig. 1*A* for a given sample. We classify the different morphologies of HRBCs as a function of $\dot{\gamma}$ in Fig. 1*B* using an in-house image-analysis program.

RBCs subjected to weak shear rates ($< 10\ s^{-1}$) commonly keep their biconcavity, similar to typical discocytes at rest (Fig. 1*A*). For $\dot{\gamma}$ increasing from 10 to 40 s^{-1} however, the percentage of discocytes decreases more than twice (Fig. 1*B*). This is due to the systematic development of two populations of cup-shaped stomatocytes: one with a circular rim and another with an elliptical one with an aspect ratio smaller than 0.95. Examples of these deformed stomatocytes are displayed in Fig. 1*A* at 18 and 40 s^{-1}, respectively. At $\dot{\gamma} = 45\ s^{-1}$, the fraction of discocytes has dramatically dropped to about 30% of the population, whereas the total amount of stomatocytes has jumped nearly to 65%. These values remain nearly constant for both cell populations up to about 400 s^{-1} (light blue region of Fig. 1*A*). However, in the region between 45 s^{-1} and 400 s^{-1}, the fraction of circular-rim-shaped stomatocytes decreases and gets replaced by the population of elliptical-rim-shaped stomatocytes with an increased ellipticity.

At $\dot{\gamma} \approx 400\ s^{-1}$ a new transition takes place. We observe a sharp increase in the population of deformed stomatocytes that seem to be strongly folded (around 475 s^{-1} in Fig. 1*B*). Most importantly, we also see the rise of a new population of RBCs showing large lobes on their surface. In most cases, we find cells with three or six lobes forming tetrahedrons, which will be henceforth referred to as trilobes or hexalobes, respectively. In the region $400\ s^{-1} < \dot{\gamma} < 2{,}000\ s^{-1}$, marked by light red in Fig. 1*B*, we observe the near disappearance of discocytes (less than 10%) and the formation of trilobes and, to a lesser degree, hexalobes, such that the polylobed RBCs represent almost 70% of the sheared population at the highest shear rates. Moreover, a rapid rise of the hexalobe population is found for $\dot{\gamma} \sim 2{,}000\ s^{-1}$, suggesting a direct correlation between the number of lobes and shear strength.

RBC Dynamics in Flow. To understand further how the acquired morphologies couple to flow and to rule out hardening artifacts we perform complementary microfluidic experiments with high-speed video microscopy at 25°C using dilute suspensions of RBCs ($Ht \approx 1\%$) in PBS/BSA (no hardening). The suspension is fed at increasing flow rates into a circular microcapillary for the same range of shear rates explored by rheometry. Local shear rate is evaluated by measuring both the local cell velocity and distance from the capillary walls. Different dynamics are detected

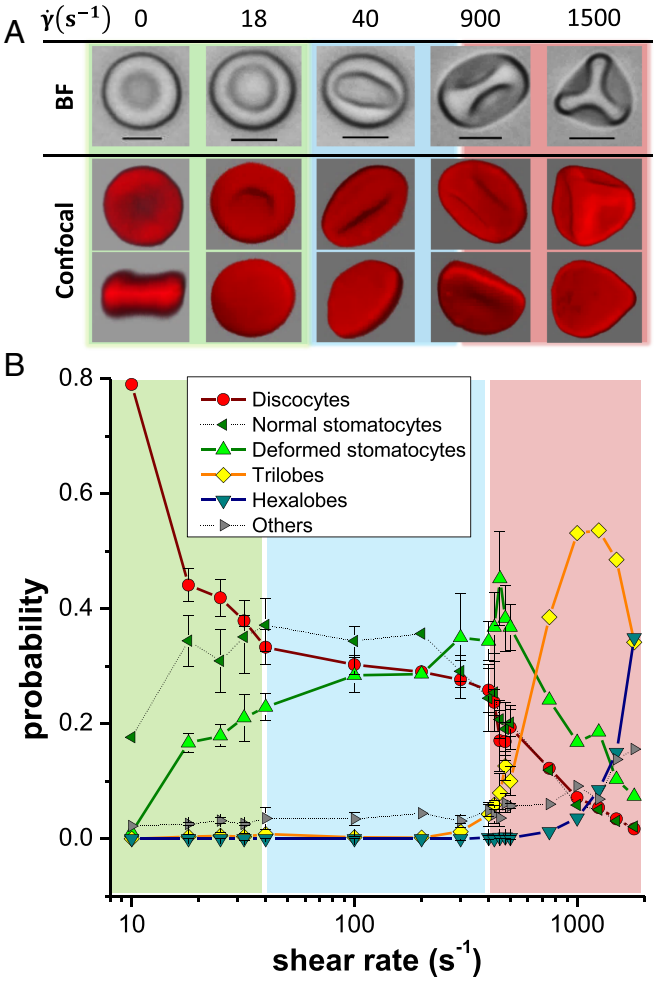

Fig. 1. Investigation of RBC shapes at different shear rates in a cone-and-plate rheometer. (*A*) Observation of hardened cells by optical (black and white) and confocal (red) microscopy: With increasing $\dot{\gamma}$ the formation of highly deformed stomatocytes and then polylobed cells (trilobe and hexalobe) is detected. (Scale bars, 5 μm.) (*B*) Shape distribution of RBC populations in samples hardened at different shear rates: the three regions in color highlight different regimes of decrease of discocyte populations. The error bars represent triplicate measurements realized in the two rapidly varying regions. They illustrate the typical variance of the measurements.

for increasing values of this estimated $\dot{\gamma}$. The time sequences shown in Fig. 2*A* are obtained in a field of view of about 300 μm long. At low shear rates ($\dot{\gamma} < 40\ s^{-1}$), the tumbling-to-rolling transition is observed, where the axis of symmetry of discocytes gradually aligns with the vorticity direction. As in the rheological setup, the number of rolling RBCs becomes significant for increasing shear rates. In addition, a substantial increase in the population of cup-shaped stomatocytes is clearly detected, which show a rolling motion in the flow as illustrated in Fig. 2*A* at $\dot{\gamma} = 150\ s^{-1}$. Moreover, observations reveal both tumbling and vacillating-breathing behaviors (Movie S1) of folded stomatocytes (Fig. 2*A*, blue box), with the latter being largely detected at high shear strengths $\dot{\gamma} > 350\ s^{-1}$ (see examples in Fig. 2 for 250 $s^{-1}$and 500 s^{-1}). Furthermore, these in vitro investigations confirm the formation and stability of polylobed shapes at higher shear rates. Two trilobes are depicted in side and top views at 750 and 800 s^{-1}, respectively, in Fig. 2*A* (light red box) and Movie S2. At such high shear rates, RBCs elongate in the vorticity direction and display three lobes that rotate around the center of mass. An even more solid-like rotation is observed for

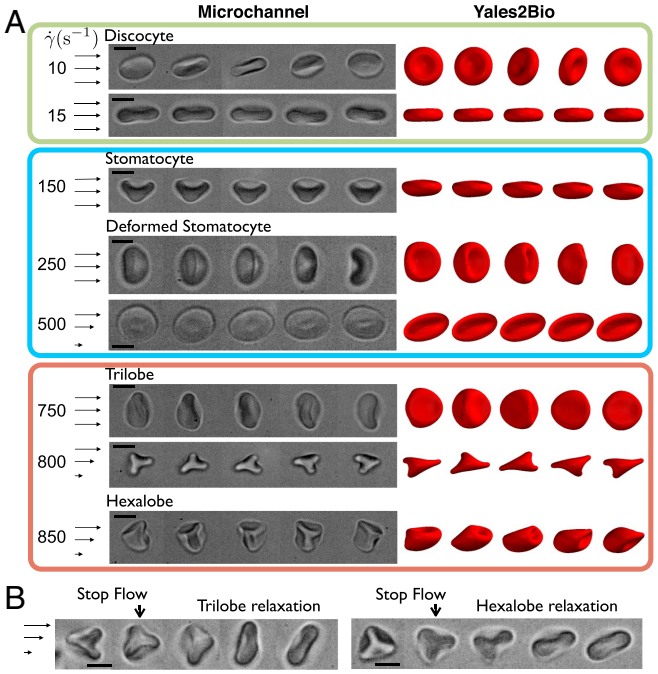

Fig. 2. Microfluidic observations of RBC dynamics in shear flow. (*A*) Sequence of RBC deformations at various $\dot{\gamma}$: time lapse = 20 ms ($\dot{\gamma} = 10\ s^{-1}$), 6 ms ($\dot{\gamma} = 15\ s^{-1}$), 3.25 ms ($\dot{\gamma} = 150, 250$, and $500\ s^{-1}$), 0.6 ms ($\dot{\gamma} = 750\ s^{-1}$), 1.75 ms ($\dot{\gamma} = 800\ s^{-1}$), and 0.6 ms ($\dot{\gamma} = 850\ s^{-1}$). The right side of the figure shows analogous time sequences of RBCs obtained with YALES2BIO simulations. Time lapses are given in $1/\dot{\gamma}$ units from top to bottom: 8, 7, 6, 6, and 7 for the four last cases. (*B*) Stop-flow sequences of (*Left*) a trilobe with a relaxation time of 1 s and intermediate images separated by 0.23 and 0.56 s and (*Right*) a hexalobe with relaxation of 1.2 s and successive images with a time interval of 0.32 and 0.71 s. (Scale bars, 5 μm.)

hexalobes under comparable flow conditions (last time sequence in Fig. 2*A* and Movie S3). These experiments show that no sharp morphological transition occurs for increasing shear rates, but rather a marked variation in shape distribution of RBC populations is present. Finally, thanks to our pressure injection system, we can produce very fast "stop flow" experiments. These experiments nicely demonstrate the dynamical nature of polylobed morphologies, because either trilobes or hexalobes return rapidly to their resting discocyte shape when the flow is stopped, as depicted in Fig. 2*B* and Movie S4. It is worth noting that the population of stomatocytes keeps its shape longer and relaxes to the discocyte population on a longer time scale of tens of minutes.

To complement the experiments we also perform numerical simulations of isolated RBCs in simple shear flow for varying shear rates, using both SDPD and YALES2BIO software (*Materials and Methods*). The simulated dynamics is presented in Fig. 2*A* using only YALES2BIO results, because agreement between the two simulations is very good. Simulations confirm the sequence of shapes and dynamics observed experimentally as well as their dependence on $\dot{\gamma}$ as shown in Fig. 2*A* and Movies S5 and S6. In comparison with experiments, simulations provide detailed information about dynamic behavior of RBCs in flow. For example, the same cell may have different stable shapes under flow (observed during several hundreds of time units $1/\dot{\gamma}$) depending on its initial orientation with respect to the flow. In particular, stomatocytes can display both rolling-like or tumbling-like motion; rolling deformed stomatocytes (Movie S5) and tumbling trilobes (Movie S6) might be found for similar shear rates. However, the sequence of shapes found experimentally seems to be qualitatively robust to moderate changes in the RBC mechanical properties, which has been tested in simulations. One difference between experimental and simulation results is hexalobed deformation of RBCs (Fig. 2*A* at the bottom), which has been observed in simulations only as a transient state. Nevertheless, in none of the simulations performed for the range $1\ s^{-1} < \dot{\gamma} < 2{,}000\ s^{-1}$ has a tank-treading ellipsoidal RBC been obtained.

Morphology and Dynamics of RBCs at High Hts. To evaluate the prevalence of polylobed shapes at physiologically relevant shear rates and Hts, similar hardening experiments were realized for several RBC suspensions with different Ht values of 5, 15, 22, 35, and 45%. $\dot{\gamma} = 900\ s^{-1}$ (at 37°C) has been selected for these experiments, because the analysis for dilute suspensions in Fig. 1*B* has shown a maximum in the population of trilobes at this shear rate. Fig. 3 indicates a significant decrease in the probability to obtain polylobed HRBCs for increasing Ht. The percentage of trilobes and hexalobes, which amounts to about 55% of the entire population at $Ht = 5\%$, is more than halved when the Ht reaches 45%. In addition, at high enough Ht many HRBCs display a deformed shape with multiple irregular lobes, making it difficult to precisely classify their morphology; these cells will be called "multilobes" and are illustrated in Fig. 3, *Lower Inset*. The fraction of these multilobed RBCs seems to be rather stable, amounting to $25\% - 35\%$ of the total population. However, the onset of a new cell morphology is detected for increasing Ht. Flattened discocytes characterized by one or several grooves or creases on their membrane have been found and are illustrated in Fig. 3, *Upper Inset* by optical and confocal microscopy. The fraction of creased discocytes increases significantly at high Ht values, amounting to almost 50% of the sample at $Ht = 45\%$. In contrast to the vast majority of polylobed RBCs in dilute suspensions, the formation of flat cells with creases is a clear effect of mutual hydrodynamic interactions between cells in such dense suspensions. Indeed, the total percentage of lobed cells with increasing Ht has the exact inverse evolution of that for creased discocytes, as shown in Fig. 3. Interestingly, physiological Hts in the microcirculation lie in the range $15 - 30\%$ (light yellow region in Fig. 3), in which a clear coexistence of different cell morphologies with a domination of lobed shapes is present.

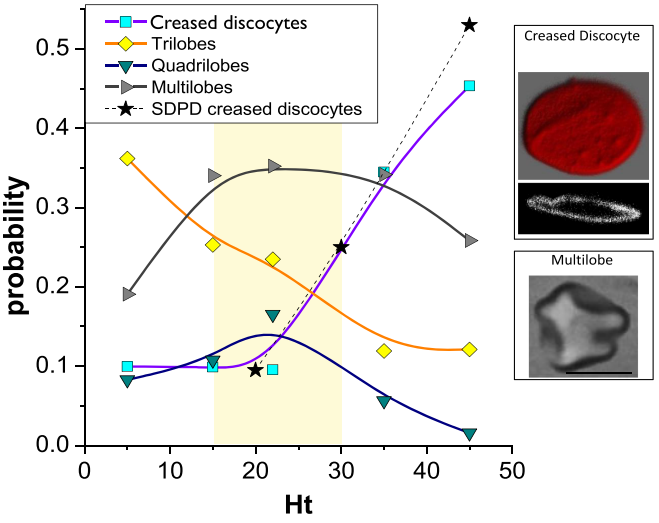

Fig. 3. Shape distributions of HRBCs at 900 s^{-1} in suspensions with different *Ht*. For clarity, discocyte and stomatocyte number densities have been omitted because they are negligible. (*Inset*) Black frames on the right, a top view and a cross-section of a creased discocyte acquired by confocal microscopy as well as an image of a multilobe in BF. Physiological Hts are indicated by the light yellow region. (Scale bar, 5 μm.)

To corroborate the existence of such folded and irregular structures in flow at high Ht we have performed SDPD simulations with dense RBC suspensions. The analysis of creased-discocyte population for different Ht is presented in Fig. 3 along with the corresponding experimental data showing a good qualitative agreement. Fig. S1 also shows RBC-extension distributions for different Ht values, which are averaged over multiple RBCs and many time instances (a typical simulation is shown in Movie S7). The extension distributions clearly show that RBCs become more stretched in the flow as Ht is increased and that at low enough Ht polylobed shapes dominate, whereas at $Ht = 45\%$ the fraction of creased discocytes becomes larger than one half. The coexistence of various cell morphologies and the evolution of different RBCs populations with increasing Ht are consistent with the observations made experimentally.

The Role of Cell Deformability in Shear-Thinning Rheograms. Now, we reexamine the interpretation of classical shear-thinning rheograms for human blood, which were introduced in the 1970s (3) and provided the seminal link between shear-induced RBC deformation, tank treading, and shear thinning. We perform experiments at $Ht = 45\%$ suspending RBCs in either PBS/BSA or their native plasma. The samples are sheared in the rheometer at 37°C (using both Couette and cone-and-plate geometry) for the range of $\dot{\gamma}$ between 5 s^{-1} and 2,000 s^{-1}. The relative viscosity (η_{rel}), defined as the ratio between the measured viscosity of the suspension (η_s) and the viscosity of the suspending medium (η_m), is obtained for different $\dot{\gamma}$. Consistent with previous work (3), at low shear rates washed blood has a significantly lower viscosity than WB because plasma induces aggregation. From $\dot{\gamma} \approx 10\ s^{-1}$, viscosity curves for both washed blood and WB merge into a common shear-thinning behavior, as shown in Fig. 4*A*. To understand the role of shape change in this regime we compare washed blood rheology with that of two HRBC suspensions at 45% Ht: one with stiff discocytes hardened at rest and the other one with polylobed cells obtained by hardening cells previously in the rheometer at $\dot{\gamma} = 1{,}500\ s^{-1}$ and resuspending them in PBS/BSA at the desired 45% Ht. Both suspensions of HRBCs show a nearly Newtonian behavior except for shear rates above 400 s^{-1}, where the onset of a slight shear-thickening is observed especially for hardened discocytes. This behavior is similar to shear thickening reported for rigid colloidal suspensions (22, 23). For both HRBC dispersions viscosity values are larger than those for washed blood; however, the sample with hardened polylobes yields a 70% lower relative viscosity than that for stiffened discocytes, as seen in Fig. 4*A*. These results indicate that from $\dot{\gamma} = 10\ s^{-1}$ up to a few hundred seconds^{-1} shear thinning is largely determined by the change in RBC dynamics from tumbling to rolling and by the deformation of RBCs into elongated stomatocytes. Beyond $\dot{\gamma} \sim 400\ s^{-1}$, however, a further viscosity drop is related to the formation of polylobed and flattened shapes discussed above.

SDPD simulations performed for $\lambda = 5$ and $Ht = 45\%$ quantitatively capture shear thinning, as shown in Fig. 4*A*. A closer look at RBCs shapes for different shear rates essentially confirms experimental observations. For moderate shear rates up to a few hundred seconds^{-1}, a prevalence of stomatocytes and multilobe cells is found, whereas at high shear rates flattened RBCs are mainly observed. Stomatocytes and polylobes found for moderate $\dot{\gamma}$ values show a tumbling-like dynamics. The dynamics of flattened RBCs at high shear rates resembles a tank-treading motion; however, these cells display persistent and dynamic membrane deformations represented by small creases or larger lobes, which continuously form and disappear. Tank treading with a steady ellipsoidal shape was never observed in simulations and the motion of flattened RBCs at high shear rates is likely to be a superposition of both cell stretching and lobe rotation.

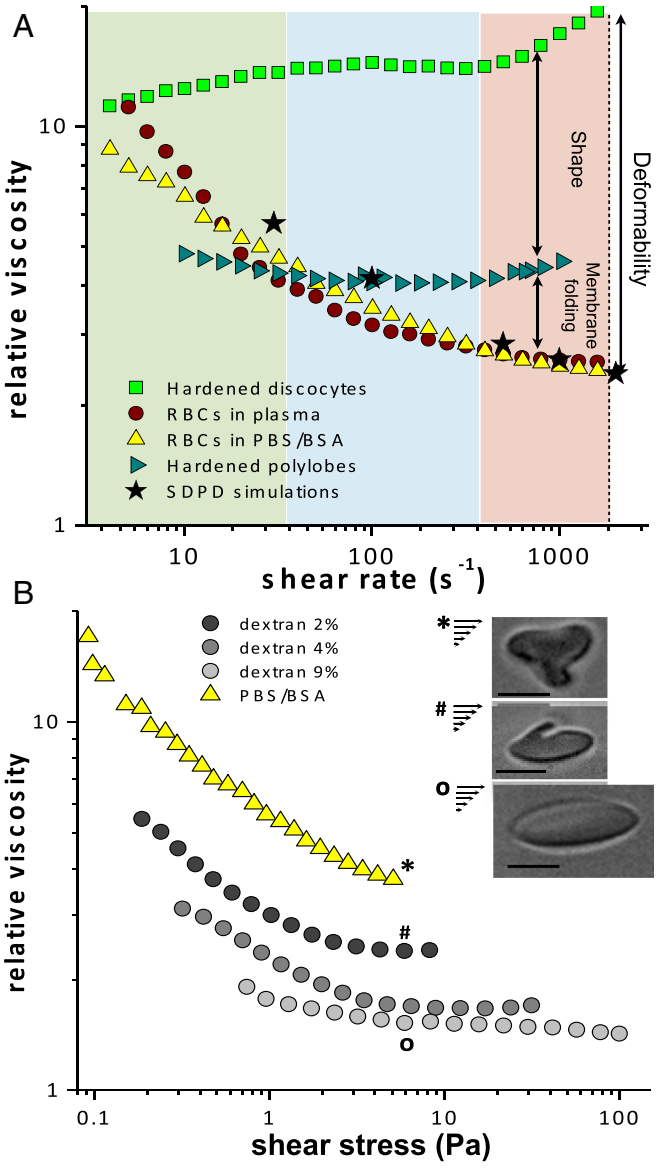

Fig. 4. Rheology of dense suspensions of RBCs ($Ht = 45\%$). (*A*) Relative viscosity of the suspensions of deformable RBCs in plasma (red) and in PBS/BSA (yellow) as a function of $\dot{\gamma}$ in comparison with the suspensions of washed cells hardened at rest (green) and at $\dot{\gamma} = 1{,}500\ s^{-1}$ (blue). Suspensions of deformable RBCs show a typical shear thinning for increasing $\dot{\gamma}$, whereas hardened samples have a nearly Newtonian behavior. SDPD simulation data (black stars) are also shown for deformable cells and agree well with the experimental results for RBCs suspended in plasma or in PBS/BSA. (*B*) Rheology of washed blood in comparison with the suspensions of RBCs in solutions with different dextran concentrations (temperature = 25 °C). (*Inset*) The effect of viscosity ratio λ is highlighted by the illustration of single cells flowing in both PBS/BSA and dextran solutions in microfluidics at a comparable shear stress τ. (Scale bars, 5 μm.)

Finally, to highlight the importance of λ for the presence of lobular shapes and their role in shear thinning in comparison with steady tank treading, we perform rheological measurements for suspensions of normal RBCs dispersed in solutions with increasing viscosities modulated by various dextran concentrations of 2%, 4%, and 9% (wt/wt) in PBS (respective viscosities: 3.4, 10.2, and 38.8 mPa·s). Ht is kept at 45% and the suspensions are sheared at 25°C for the range of $\dot{\gamma}$ between 10 s^{-1} and 2,000 s^{-1} (without hardening). Fig. 4*B* presents relative viscosities of these suspensions as a function of the shear

stress τ ($= \eta_s \dot{\gamma}$). The curves for PBS/BSA and 9% dextran solution display inconsistent trends. In PBS/BSA, which corresponds to high viscosity ratios ($\lambda \approx 10$ at 25°C), a significant and continuous decrease of η_{rel} is observed for increasing τ up to the rheometer limit of about 6 Pa. In contrast, 9% dextran suspensions ($\lambda \approx 0.25$) exhibit a slight shear thinning for stresses close to 1 Pa, but η_{rel} yields a plateau for higher stresses (Fig. 4*B*). Samples with 2% and 4% dextran solutions show an intermediate behavior, in which the occurrence of an increasingly significant shear thinning for increasing λ is detected. In parallel, we have performed microfluidic observations of single RBCs flowing in 2% and 9% dextran solutions at $Ht = 1\%$ for comparable shear stresses. Contrary to the behavior of RBCs in PBS/BSA, cells in 9% dextran solutions do not assume polylobed shapes but show a rather sharp transition from rigid tumbling discocytes to tank-treading ellipsoids that elongate with increasing stresses. This transition takes place at $\tau \sim 1 Pa$, which is consistent with the change in slope of the corresponding η_{rel} curve in Fig. 4*B*. In Fig. 4*B*, *Inset* an illustration of the effect of λ on RBC dynamics is presented. Images show the shapes of cells dispersed respectively in PBS/BSA and 2% and 9% dextran solutions and flowing in a microchannel with the same estimated local shear stress of $\tau = 6$ Pa. A decrease in λ promotes in-flow orientation, elongation, and simultaneous reduction of lobe size (Movie S8). When $\lambda \approx 0.25$, polylobed cells are completely replaced by elongated tank-treading ellipsoids (Fig. 4*B*, *Inset*). It is noteworthy that all images in Fig. 4*B*, *Inset* and movies in *Supporting Information* refer to RBCs flowing in microchannels in which the presence of a gradient in $\dot{\gamma}$ can potentially affect RBC dynamics, whereas rheological measurements were performed under pure shear flow conditions. However, comparison between off-center shape sequences in 50-μm capillaries and simple-shear YALES2BIO simulations presented in Fig. 2*A* indicates a rather marginal effect of the gradient of shear rate.

Discussion

Without aggregation, blood continuous shear thinning is the result of a rich dynamical behavior of RBC population, based primarily on the inability of RBCs to tank-tread under physiological conditions ($\lambda \approx 5$). In this study, we have observed a diversity of shapes and dynamical states of RBCs for increasing shear rates and the development of a large fraction of highly deformed and polylobed cells for $\dot{\gamma} > 400$ s^{-1} (Figs. 1 and 2), which has been confirmed by simulations.

For single cells in dilute suspensions, and for $\dot{\gamma} < 1$ s^{-1}, the biconcave shape is preserved and RBCs behave like rigid oblate ellipsoids, such that the membrane and the enclosed fluid rotate as a rigid body. For increasing shear rates up to 10 s^{-1}, more and more cells are found to roll on their edge, as previously observed in experiments using rheoscopes (24) and more recently in flow chambers (18, 25). Shear thinning in this range of shear rates is therefore mainly controlled by discocyte orientation. Rolling has its origin in shear elasticity of the membrane. Under physiological conditions, membrane tank treading is forbidden due to the relatively high internal viscosity as predicted by viscous ellipsoidal models of the RBC (26). However, during each tumbling period the membrane elements oscillate around a given position and this local oscillatory strain seems to destabilize RBCs from tumbling toward rolling (27) instead of tank treading. Although not fully settled, this phenomenon is well captured by our simulations and is described as a stable motion in several recent numerical simulations of capsules (28) and RBCs (29).

In the range of shear rates between 45 and 400 s^{-1}, a large population of the rolling discocytes loses one dimple and become rolling stomatocytes, displaying at first more frequently a circular rim up to 45 s^{-1} and then a breathing elliptical rim for shear rates reaching 400 s^{-1}. In this second morphological transition, rolling stomatocytes are showing a smaller cross-section to shear flow than rolling discocytes, reducing their disturbances of the streamlines. This leads to a further shear thinning. Both our numerical approaches capture this flow-induced morphological transition for single RBCs. The loss of the dimple happens abruptly in simulations highlighting a buckling instability, which is also confirmed experimentally by the long time scales (minutes) necessary for the population of stomatocytes to relax to a discocyte shape.

Beyond 400 s^{-1} the dilute population of RBCs is subjected to a new shift in morphology and large lobes develop on the surface of the cells (Fig. 1*A*). These out-of-plane deformations are again a signature for a lack of fluidization of the membrane even for the largest stress of 6 Pa we were able to reach both experimentally (with the rheometer and in microflows) and numerically. Noteworthy, Sutera and Mehrjardi (30) studied in the 1970s the morphology of cells hardened in PBS solutions at very high shear stresses ($\tau \geq 10$ Pa). Their images at $\tau = 10$ Pa show the presence of pronounced concavities on RBCs similar to those we observe for polylobed cells. Our experiments confirm how lobes are directly associated with a large enough viscosity contrast λ because they vanish in very viscous dextran solutions, as shown in Fig. 4 (from $\lambda \approx 2.9$). However, the exact nature of these transitions and the development of folded shapes remain to be understood. Modifications of an RBC membrane at rest can also induce similar transformations observed here for increasing shear rates. Theoretically, a large equilibrium-shape variety has been obtained for RBCs including stomatocytes, with circular and deformed rims, and trilobes (named knizocytes in the literature), by changing the resting elastic state of the cytoskeleton and the area difference between lipid leaflets in the model (31). Despite this striking similarity, the dynamic shapes in our simulations have been observed without any explicit modification of the membrane. These results open the road for further experimental investigations on the possible flow-induced modifications of RBCs membrane and their impact on dynamics.

Our dilute single-cell experiments and simulations show how out-of-plane deformations are inevitable for increasing shear rates. However, for more concentrated suspensions, a large population of creased and flattened discocytes appears both in experiments (Movie S9) and simulations (Movie S7 and Fig. S1). Although it is perfectly conceivable that large lobes cannot easily develop on membranes in crowded suspensions, the complex flow between cells seems to counterbalance the inherent tendency of RBCs to elongate more in the vorticity direction. It is this fine balance between vorticity- and flow-direction elongations that aligns cells on average parallel to the flow. Nevertheless, any variations in relative positions between the cells or any collisions immediately give birth to local bulges on the membranes and produce large fluctuations of shapes as seen in RBC extension distributions (Movie S7 and Fig. S1).

In summary, blood shear thinning is related to a rich behavior of RBCs in shear flow convoluted with a large distribution of cell shapes for any given flow condition. The lack of membrane fluidity for high viscosity contrast is the key feature that controls RBCs' behavior. Besides shear thinning, several fundamental physiological phenomena have been analyzed under the assumption of membrane tank treading, such as vasoregulatory ATP release by RBCs in strong shear flows (32) or the formation of a few-micron-thick cell-free layer adjacent to the vessels walls that is responsible for the apparent viscosity drop with decreasing vessel diameter, the so-called Fåhræus–Lindqvist effect (33). Our study questions the relevance of such droplet-like analogy for RBC dynamics to explain these phenomena and seeks to reexplore them both experimentally and theoretically for physiologically relevant viscosity and stress conditions. Finally, our study suggests that in pathological states inducing a change in blood

features such as plasma composition, RBC cytosol viscosity, or membrane mechanical properties the onset of shape transitions will be affected, and this should play a central role in pathological blood rheology and flow.

Materials and Methods

Blood Samples. Nonclinically issued RBCs for laboratories have been obtained from blood bags (that cannot be used for donation) through the local blood bank (Etablissement Français du Sang, Montpellier, France). Sample preparation and characteristics are given in *Supporting Information* as well as experiments, summarized in Table S1.

Rheology and Imaging. Rheology experiments were performed in cone-plate and Couette geometries with a stress-imposed rheometer (AR 2,000; TA Instruments) at constant temperature. Dilute and semidilute cell suspensions were rigidified in flow by adding a high-glutaraldehyde concentration solution in small volume during flow. Such an amount of glutaraldehyde produces a very rapid, strong, and permanent solidification. Both shearing and hardening were carried out within 2 min. Samples were then collected, washed, and suspended in PBS solution for microscopic examination realized both in BF and with confocal microscopy. See details in *Supporting Information*.

Microfluidics and Imaging. Microflow observations were realized at 25°C in glass round capillaries with a diameter of 50 μm. Flow rates were adjusted by a OB1 Pressure Controller (ElveFlow) operating up to 2 bar. Images were acquired at a high magnification (60× and 100× objectives) on a Nikon inverted microscope equipped with a high-speed camera Phantom Miro M320S (Vision Research) and subsequently analyzed by a custom image analysis software (ImageJ). See details in *Supporting Information*.

Numerical Simulations. Two different in-house softwares were used for numerical simulations. The first one, YALES2BIO (19, 34), is a finite-volume parallel solver for the incompressible Navier–Stokes equations on unstructured meshes. Fluid-structure coupling was implemented using an immersed boundary method adapted to unstructured grids (19). The second one, the SDPD method (21), is a mesoscale hydrodynamic particle-based approach that represents fluid flow, and a RBC membrane is modeled as a triangulated network of springs (20) whose vertices are coupled to the fluid via frictional forces (20). Further details about the numerical methods and setups can be found in *Supporting Information*.

ACKNOWLEDGMENTS. S.M. and F.N. thank Dr. Moureau and Dr. Lartigue (CORIA, UMR 6614) and the SUCCESS scientific group for providing the YALES2 code, which served as a basis for the development of YALES2BIO Catherine Braun Breton is acknowledged for her help with blood-sample manipulation. This work was supported by the Oséo-Banque Publique d'Investissement project Dat@Diag (M.A., S.M., F.N., and L.L.), Labex Numev Convention ANR-10-LABX-20 (M.A. and L.L.), and Agence Nationale de la Recherche (ANR) Grant ANR-11-JS09-0011 (to S.M. and F.N.). Simulations with YALES2BIO were performed using HPC resources from Grand Equipement National de Calcul Intensif - Centre Informatique National de l'Enseignement Supérieur (Grant 2016-c2016037194). D.A.F. acknowledges funding by the Alexander von Humboldt Foundation. SDPD simulations were performed using a central processing unit time allocation at the Jülich Supercomputing Center.

1. Wells RE, Merrill EW (1961) Shear rate dependence of the viscosity of whole blood and plasma. *Science* 133:763–764.
2. Dintenfass L (1968) Internal viscosity of the red cell and a blood viscosity equation. *Nature* 219:956–958.
3. Chien S (1970) Shear dependence of effective cell volume as a determinant of blood viscosity. *Science* 168:977–979.
4. Brust M, et al. (2013) Rheology of human blood plasma: Viscoelastic versus Newtonian behavior. *Phys Rev Lett* 110:078305.
5. Merrill EW, Gilliland ER, Lee TS, Salzman EW (1966) Blood rheology: Effect of fibrinogen deduced by addition. *Circ Res* 18:437–446.
6. Qin Z, Durand LG, Allard L, Cloutier G (1998) Effects of a sudden flow reduction on red blood cell rouleau formation and orientation using RF backscattered power. *Ultrasound Med Biol* 24:503–511.
7. Fedosov DA, Pan W, Caswell B, Gompper G, Karniadakis GE (2011) Predicting human blood viscosity in silico. *Proc Natl Acad Sci USA* 108:11772–11777.
8. Lipowsky HH (2005) Microvascular rheology and hemodynamics. *Microcirculation* 12:5.
9. Popel AS, Johnson PC (2005) Microcirculation and hemorheology. *Annu Rev Fluid Mech* 37:43–69.
10. Wells R, Schmid-Schönbein H (1969) Red cell deformation and fluidity of concentrated cell suspensions. *J Appl Physiol* 27:213–217.
11. Diez-Silva M, Dao M, Han J, Lim CT, Suresh S (2010) Shape and biomechanical characteristics of human red blood cells in health and disease. *MRS Bull* 35:382.
12. Goldsmith HL, Marlow J (1972) Flow behaviour of erythrocytes. I. Rotation and deformation in dilute suspensions. *Proc R Soc B* 182:351–384.
13. Fischer TM, Stöhr-Lissen M, Schmid-Schönbein H (1978) The red cell as a fluid droplet: Tank tread-like motion of the human erythrocyte membrane in shear flow. *Science* 202:894–896.
14. Abkarian M, Faivre M, Viallat A (2007) Swinging of red blood cells under shear flow. *Phys Rev Lett* 98:188302.
15. Sutera SP, Pierre P, Zahalak G (1989) Deduction of intrinsic mechanical properties of the erythrocyte membrane from observations of tank-treading in the rheoscope. *Biorheology* 26:177–197.
16. Korin N, Bransky A, Dinnar U (2007) Theoretical model and experimental study of red blood cell (RBC) deformation in microchannels. *J Biomech* 40:2088–2095.
17. Fischer TM, Schmid-Schönbein H (1977) Tank tread motion of red-cell membranes in viscometric flow-behavior of intracellular and extracellular markers (with film). *Red Cell Rheology* (Springer, New York), pp 347–361.
18. Dupire J, Socol M, Viallat A (2012) Full dynamics of a red blood cell in shear flow. *Proc Natl Acad Sci USA* 109:20808–20813.
19. Mendez S, Gibaud E, Nicoud F (2014) An unstructured solver for simulations of deformable particles in flows at arbitrary Reynolds numbers. *J Comput Phys* 256:465.
20. Fedosov DA, Caswell B, Karniadakis GE (2010) A multiscale red blood cell model with accurate mechanics, rheology, and dynamics. *Biophys J* 98:2215–2225.
21. Müller K, Fedosov DA, Gompper G (2015) Smoothed dissipative particle dynamics with angular momentum conservation. *J Comput Phys* 281:301–315.
22. Barnes HA (1989) Shear-thickening (dilatancy) in suspensions of non aggregating solid particles dispersed in newtonian liquids. *J Rheol* 33:329–366.
23. Brown E, et al. (2011) Shear thickening and jamming in densely packed suspensions of different particle shapes. *Phys Rev E Stat Nonlin Soft Matter Phys* 84:1–11.
24. Bitbol M (1986) Red blood cell orientation in orbit C= 0. *Biophys J* 49:1055–1068.
25. Yao W, et al. (2001) Low viscosity ektacytometry and its validation tested by flow chamber. *J Biomech* 34:1501–1509.
26. Keller SR, Skalak R (1982) Motion of a tank-treading ellipsoidal particle in a shear flow. *J Fluid Mech* 120:27–47.
27. Dupire J, Abkarian M, Viallat A (2015) A simple model to understand the effect of membrane shear elasticity and stress-free shape on the motion of red blood cells in shear flow. *Soft Matter* 11:8372–8382.
28. Dupont C, Salsac AV, Barthès-Biesel D (2013) Off-plane motion of a prolate capsule in shear flow. *J Fluid Mech* 725:180–198.
29. Cordasco D, Bagchi P (2013) Orbital drift of capsules and red blood cells in shear flow. *Phys Fluids* 25:091902.
30. Sutera SP, Mehrjardi MH (1975) Deformation and fragmentation of human red blood cells in turbulent shear flow. *Biophys J* 15:1–10.
31. Lim GHW, Wortis M, Mukhopadhyay R (2002) Stomatocyte-discocyte-echinocyte sequence of the human red blood cell: Evidence for the bilayer-couple hypothesis from membrane mechanics. *Proc Natl Acad Sci USA* 99:16766–16769.
32. Forsyth AM, Wan J, Owrutsky PD, Abkarian M, Stone HA (2011) Multiscale approach to link red blood cell dynamics, shear viscosity, and ATP release. *Proc Natl Acad Sci USA* 108:10986–10991.
33. Fåhræus R, Lindqvist T (1931) The viscosity of the blood in narrow capillary tubes. *Am J Physiol* 96:562–568.
34. Gibaud E (2015) Numerical simulation of red blood cells flowing in a blood analyzer. PhD thesis (Université de Montpellier, Montpellier, France).
35. Dulinska I, Targosz M, Strojny W, Lekka M, Czuba P, Balwierz W, Szymonski M (2006) Stiffness of normal and pathological erythrocytes studied by means of atomic force microscopy. *J Biochem Biophys Methods* 66:1–11.
36. Dodson III WR, Dimitrakopoulos, P Tank-treading of erythrocytes in strong shear flows via a nonstiff cytoskeleton-based continuum computational modeling. *Biophys J* 99:2906–2916, 2010.
37. Cordasco DY, Bagchi P (2014) Comparison of erythrocyte dynamics in shear flow under different stress-free configurations. *Phys Fluids*, 26:041902.
38. Evans EA, Fung YC (1972) Improved measurements of the erythrocyte geometry. *Microvasc Res*4:335–347.
39. Plimpton S (1995) Fast parallel algorithms for short-range molecular-dynamics. *J Comput Phys* 117:1–19.
40. Español P, Revenga M (2003) Smoothed dissipative particle dynamics. *Phys Rev E Stat Nonlin Soft Matter Phys* 67:026705.
41. Groot RD, Warren PB (1997) Dissipative particle dynamics: Bridging the gap between atomistic and mesoscopic simulation. *J Chem Phys* 107:4423.
42. Fedosov DA, Peltomaeki M, Gompper G (2014) Deformation and dynamics of red blood cells in flow through cylindrical microchannels. *Soft Matter* 10:4258–4267.